Journal of Biomedical Optics

SPIEDigitalLibrary.org/jbo

Targeted detection of murine colonic dysplasia in vivo with flexible multispectral scanning fiber endoscopy

Sharon J. Miller
Cameron M. Lee
Bishnu P. Joshi
Adam Gaustad
Eric J. Seibel
Thomas D. Wang

Targeted detection of murine colonic dysplasia in vivo with flexible multispectral scanning fiber endoscopy

Sharon J. Miller,[a] Cameron M. Lee,[b] Bishnu P. Joshi,[a] Adam Gaustad,[c] Eric J. Seibel,[b] and Thomas D. Wang[a,c]
[a]University of Michigan, Department of Internal Medicine, Division of Gastroenterology, 109 Zina Pitcher Pl. BSRB 1522, Ann Arbor, Michigan 48109-2200
[b]University of Washington, Department of Mechanical Engineering, Human Photonics Laboratory, Box 352600, Seattle, Washington 98195
[c]University of Michigan, Department of Biomedical Engineering, Division of Gastroenterology, 109 Zina Pitcher Pl. BSRB 1522, Ann Arbor, Michigan 48109-2200

Abstract. Gastrointestinal cancers are heterogeneous and can overexpress several protein targets that can be imaged simultaneously on endoscopy using multiple molecular probes. We aim to demonstrate a multispectral scanning fiber endoscope for wide-field fluorescence detection of colonic dysplasia. Excitation at 440, 532, and 635 nm is delivered into a single spiral scanning fiber, and fluorescence is collected by a ring of light-collecting optical fibers placed around the instrument periphery. Specific-binding peptides are selected with phage display technology using the *CPC;Apc* mouse model of spontaneous colonic dysplasia. Validation of peptide specificity is performed on flow cytometry and in vivo endoscopy. The peptides KCCFPAQ, AKPGYLS, and LTTHYKL are selected and labeled with 7-diethylaminocoumarin-3-carboxylic acid (DEAC), 5-carboxytetramethylrhodamine (TAMRA), and CF633, respectively. Separate droplets of KCCFPAQ-DEAC, AKPGYLS-TAMRA, and LTTHYKL-CF633 are distinguished at concentrations of 100 and 1 μM. Separate application of the fluorescent-labeled peptides demonstrate specific binding to colonic adenomas. The average target/background ratios are 1.71 ± 0.19 and 1.67 ± 0.12 for KCCFPAQ-DEAC and AKPGYLS-TAMRA, respectively. Administration of these two peptides together results in distinct binding patterns in the blue and green channels. Specific binding of two or more peptides can be distinguished in vivo using a novel multispectral endoscope to localize colonic dysplasia on real-time wide-field imaging. [DOI: 10.1117/1.JBO.17.2.021103]

Keywords: multispectral; endoscopy; colon; wide-field; fluorescence; peptide; dysplasia; cancer.

Paper 11329SS received Jun. 29, 2011; revised manuscript received Sep. 17, 2011; accepted for publication Sep. 21, 2011; published online Mar. 12, 2012.

1 Introduction

The early detection and prevention of colorectal cancer is currently being performed with screening colonoscopy, where polypoid adenomas are identified and removed. However, a number of clinical studies have shown a significant miss rate of >20% for the detection of these grossly visible lesions.[1–3] Furthermore, non-polypoid (flat and depressed) dysplasia may represent over 25% of all adenomas and may confer a higher risk for malignancy.[4–7] Improvements in image contrast for visualizing these pre-malignant lesions may result in reduced mortality and better outcomes.[8] Molecular imaging is a powerful tool for detecting and guiding therapy for early cancer, as it can rapidly assess protein expression patterns on the surface of cells transforming into malignancy.[9] These molecular changes often occur prior to any detectable morphological abnormality. Detecting targets of dysplasia on wide-field imaging in real time is needed to localize these pre-malignant lesions and to guide intervention.

Colorectal cancer can present with multiple overexpressed cell surface targets, such as epidermal growth-factor receptor (EGFR), epithelial cell adhesion molecule (EpCAM), mucin (MUC1), matrix metalloproteinases (MMPs), etc.,[10,11] that in theory can be visualized using highly specific molecular probes during surveillance endoscopy to guide tissue biopsy, assess for sub-mucosal invasion, and monitor response to therapy. Activatable probes emit fluorescence in the presence of molecular targets and include proteolytic enzymes,[12] MMPs,[13] endothelial-specific markers,[14] and apoptosis reporters.[15,16] However, these agents have not been translated into the clinic in part due to limitations in delivery, pharmacokinetics, and immunogenicity. Peptides have been demonstrated in the clinic[17] and are attractive targeting moieties because of their small size, minimal immunogenicity, and rapid binding kinetics. In addition, they are easily labeled with multiple fluorophores. With topical application to the mucosa, we have previously demonstrated that peptides derived from phage display technology can preferentially bind to diseased mucosa in the esophagus[18] and colon.[19]

Current wide-field imaging methods being developed as an adjunct to conventional endoscopy for the early detection of colorectal cancer include narrow band imaging (NBI), chromoendoscopy, and autofluorescence imaging. NBI relies on enhanced contrast from vasculature by enhancing hemoglobin absorption, allowing diseased tissue to appear darker in color than surrounding normal mucosa.[20,21] Clinical studies have reported that NBI alone may not aid in detection of dysplasia and still requires white light endoscopy for guiding tissue biopsy.[22] Chromoendoscopy utilizes non-specific exogenous dyes, such as indigo carmine, to enhance micro-anatomical changes in the mucosa.[23] Like NBI, chromoendoscopy relies on white light endoscopy for

Address all correspondence to: Thomas D. Wang, University of Michigan, Department of Biomedical Engineering, Division of Gastroenterology, 109 Zina Pitcher Pl. BSRB 1522, Ann Arbor, Michigan 48109-2200. Tel: +734 936 1228; Fax: +734 647 7950; E-mail: thomaswa@umich.edu

0091-3286/2012/$25.00 © 2012 SPIE

guided tissue biopsy and may miss flat lesions that do not present sufficient contrast in topographical changes of the epithelium. Autofluorescence imaging is sensitive to endogenous fluorescence from molecules such as collagen, NADH, FAD, and porphyrins.[24] Debris and mucosal folds that cause shadows can also limit the specificity of this approach.[25] To be accepted by the medical community, a novel instrument must improve current imaging capabilities while being used in tandem with conventional white light endoscopy.

The scanning fiber endoscope is an ultrathin, flexible instrument that has been developed for collecting color images from Barrett's esophagus and peripheral airways for early detection of cancer with minimal invasiveness.[26] This system scans red, green, and blue (RGB) laser beams in a spiral pattern on the tissue surface, and backscattered (reflectance) light is collected by a ring of optical fibers.[27] Thus, images with sub-cellular resolution and large fields-of-view (FOV) can be collected by actively scanning the incident beam, rather than passively detecting with a camera using an endoscope-compatible instrument. The aim of this study is to demonstrate a novel, integrated methodology using a multispectral scanning fiber endoscope to collect wide-field fluorescence images in vivo from multiple peptides that bind specifically to colonic dysplasia. We use a genetically engineered mouse model of spontaneous colorectal cancer based on somatic *Apc* gene inactivation.[28] This novel, targeted imaging strategy has the potential to significantly impact early detection and treatment of colorectal cancer by imaging multiple overexpressed gene targets simultaneously, and it can be generalized for use in other hollow organs, such as the biliary tract, esophagus, lung, and stomach.

2 Methods

2.1 *Multispectral Scanning Fiber Endoscope*

A scanning fiber endoscope system was adapted for fluorescence detection in three channels (RGB) using excitation at 440 (NDHB510APA, Nichia, Tokyo, Japan), 532 (FTEC532-V10TA0, Blue Sky Research, Milpitas, CA), and 635 (FMXL635-017TA0B, Blue Sky Research) nm using an RGB coupler (OZ Optics, Ottawa, Canada).[29] The three laser sources are delivered simultaneously into the scanning fiber and focused to the same point on the illumination plane using a custom lens assembly,[27] as shown in the schematic in Fig. 1(a). The laser power coming out of the distal tip of the endoscope is <2 mW for each channel, a level consistent with a non-significant risk (NSR) determination by the US Food and Drug Administration (FDA, 21 CFR 812) for future human clinical studies. We reduced the amplitude of the spiral scanner to achieve a divergence angle of 70 deg (max 100 deg) to minimize noise in the periphery of the image.[26] Fluorescence is collected by a ring of 12 step-index plastic optical fibers (POF) with numerical aperture (N.A.) of 0.63 and outer diameter of 250 μm (Toray Industries Inc., Tokyo, Japan).

The detection system, shown in Fig. 1(b), uses longpass ($\lambda_{LP} = 450$ nm) and notch ($\lambda_{N1} = 532$ nm and $\lambda_{N2} = 632.8$ nm) filters (Edmund Optics Inc., Barrington, NJ) to reject the reflectance component (RGB laser excitation) of the light emerging from the collection fibers. The fluorescence component is deflected into three individual channels using dichroic beam splitters DM1 ($\lambda_c = 460$ nm) and DM2 ($\lambda_c = 550$ nm) (Chroma Technology Corp, Bellows Falls, VT). An additive RGB set of dichroics ($\lambda_{R,G,B}$, part# 52–546, Edmund Optics Inc.) is used to filter the individual fluorescence beams, which are focused onto separate PMT (H7826-01, Hamamatsu Corp, Hamamatsu City, Japan) detectors using an objective lens ($O_{R,G,B}$, $f = 25$ mm, N.A. $= 0.46$ The PMT signals are sampled at 25 MHz to generate video rate (30 Hz) images.

2.2 *Peptide Selection and Validation*

Cell culture reagents were purchased from Invitrogen (Carlsbad, CA). Chemical reagents were purchased from Sigma-Aldrich (St. Louis, MO) unless otherwise noted. Mice were cared for under the approval of the University Committee on the Use and Care of Animals (UCUCA) at the University of Michigan. Five- to seven-month-old *CPC;Apc* mice that have a Cre-regulated somatic mutation in one *Apc* allele, causing adenomas to develop spontaneously in the distal colon at approximately three months of age, were used. This mutation is commonly found in sporadic human colorectal cancer.[30] All mice were housed in specific pathogen-free conditions and supplied water ad libitum throughout the study. Peptide selection was performed with in vivo phage display technology using this mouse as the biopanning substrate (Appendix Methods). Specific binding of the candidate peptides to primary dysplastic colonic epithelial cells were validated on flow cytometry ex vivo and with small animal endoscopy in vivo using FITC-labeled peptides using a nonscanning white light endoscope.[19]

2.3 *Peptide Synthesis*

The target and control peptides were prepared using solid phase synthesis with standard Fmoc chemistry. Fmoc protected *L*-amino acids were used, and synthesis was assembled on rink amide MBHA resin using a PS3 (Protein Technologies, Inc., AZ) automatic peptide synthesizer. The candidate peptides for the validation study were labeled with 5′-FITC (Anaspec, Fremont, CA) at the C-terminus on the side chain of a lysine residue via a GGGSK linker. The candidate peptides for the multispectral study were labeled with three different organic fluorophores. 7-Diethylaminocoumarin-3-carboxylic acid (DEAC, Sigma-Aldrich, St. Louis, MO) has a peak absorption and emission at 432 and 472 nm, respectively. 5-Carboxytetramethylrhodamine (TAMRA, Chempep, Wellington, FL) has a peak absorption and emission at 541 and 568 nm, respectively. CF633 (Biotium Inc., Hayward, CA) has a peak absorption and emission at 630 and 650 nm, respectively. These dyes have peak absorption that approximately match the laser sources. In addition, the peptide GGGAGGGAGGGK was used as a control.

2.4 *Fluorescence Spectra from Multiple Peptides*

A fiber-coupled spectrophotometer (Ocean Optics, Dundin, FL) was used to validate the excitation and emission spectra of the fluorescent-labeled peptides. Droplets of each fluorescent-labeled peptide at 1 μM concentration were analyzed individually. The optical collection fibers of the multispectral scanning fiber endoscope were disconnected from the base station and connected to the spectrophotometer. Directed data collection was performed by stopping the motion of the scanning fiber and aiming the illumination spot at the droplet. Readings were then acquired using a 3 ms integration time with Ocean Optics Spectra Suite software.

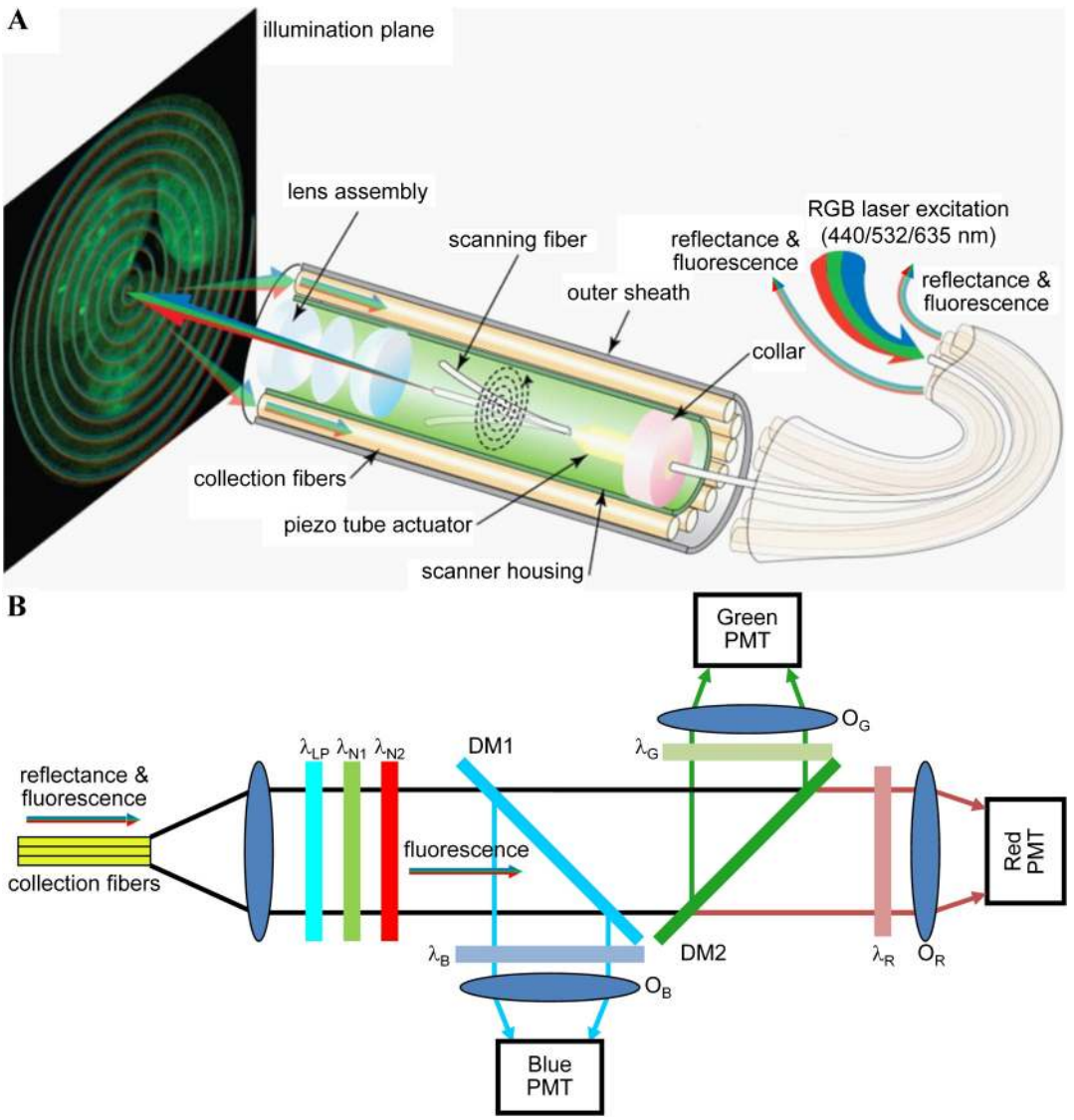

Fig. 1 Multispectral scanning fiber endoscope. (a) Optical design. RGB laser excitation (440, 532, and 635 nm) is delivered into a single-mode optical fiber that is scanned in a spiral pattern by a piezo tube actuator and focused on to the tissue (illumination plane) by a lens assembly. Fluorescence is collected by a ring of 12 collection fibers mounted around the periphery of the scanner housing, protected by an outer sheath. (b) Fluorescence detection. Reflectance from RGB laser excitation is removed using a combination of longpass ($\lambda_{LP} = 450$ nm) and notch ($\lambda_{N1} = 532$ nm and $\lambda_{N2} = 632.8$ nm) filters. Fluorescence is deflected into individual RGB channels using dichroic mirrors DM1 ($\lambda_C = 460$ nm) and DM2 ($\lambda_C = 550$ nm) and an additive dichroic filter set (λ_R, λ_G, and λ_B) prior to detection with PMTs.

2.5 *Individually and Combined Targeted In Vivo Images*

The *CPC;Apc* mice were first imaged with white light using a nonscanning endoscope (Karl Storz Veterinary Endoscopy, Goleta, CA) to assess for the presence of colonic adenomas that have a diameter between ~0.5 and 4 mm.[19] If found, the adenomas were rinsed of debris, including stool and mucous, by delivering tap water through a 3 Fr instrument channel. Then the fluorescent-labeled peptides were delivered topically at a concentration of 100 μM in $1 \times$PBS in a volume of 1 mL to the distal 4 cm of the colon and rectum. The peptides were incubated for 5 min, and then the unbound peptides were rinsed away with tap water three times. The colon was inspected for any residual peptide, and when clean, the colon was insufflated with air and imaged with the multispectral scanning fiber endoscope. Cre-recombinase negative littermates that do not express colonic adenomas were used as controls.

Videos collected during endoscopy were exported as avi video files and converted into sequential png images using Apple QuickTime. White light and fluorescence images for each adenoma were analyzed in NIH Image J. The white light image was utilized to draw a region of interest (ROI) around the adenoma or adjacent normal appearing colonic mucosa, which was then superimposed onto the fluorescence image. The mean fluorescence intensities were calculated for each ROI, and a target/background (T/B) ratio was calculated for each colonic adenoma and compared to the surrounding normal appearing mucosa.

2.6 *Statistical Analysis*

All results are shown as mean $\pm$ one standard deviation. After data normality was established using the Shapiro-Wilk test, two-sided independent sample t-tests were performed to determine statistical significance (significance level defined as

$\alpha = 0.05$) between the target and control peptides for specific binding to colonic adenomas (PASW Statistics 18, Chicago, IL).

3 Results

3.1 *Multispectral Scanning Fiber Endoscope*

The en face (top) and side-view (bottom) of distal tip of the flexible multispectral endoscope (1.6 mm outer diameter) is shown in Fig. 2(a). The distal end of the single illumination optical fiber is scanned in 250 circles in a growing spiral pattern at approximately 11.5 kHz. This scanning strategy can be appreciated by the faint spiral of periodic noise from laser reflectance off the cover glass in Figs. 2(b) and 2(c). Real-time zooming to the diffraction limit of the optics can be performed by reducing the scan angle while capturing the same number of pixels over the FOV.[29] The sub-millimeter lens assembly[27] seals the distal tip of the instrument and extends the waist of the laser beam to define a depth of focus that ranges between 2 and 50 mm. We achieved a spatial resolution of <15 μm at a distance of 3 mm from the distal tip to the illumination plane and <1 mm at the maximum depth of focus. This unique combination of scanning mechanism and optics allows for a flexible instrument to be realized in a much smaller package yet match the high-quality images from standard medical endoscopes.

3.2 *Peptide Selection and Validation*

After three rounds of in vivo phage biopanning that included heart perfusion as a method for clearing nonspecific vascular binders, the preference of the phage pools collected during all rounds of biopanning indicated that the phages were binding more specifically to colonic adenomas in comparison to normal appearing adjacent colonic mucosa, kidney, and liver [Fig. 3(a)]. Phages that bound to colonic adenomas approximately 10 times greater in number than to normal appearing colonic mucosa were chosen. As a result, 42 individual phage clones were sequenced from the third round of biopanning and were individually amplified and conjugated to 5′-FITC. Binding to isolated colonic epithelial cells from adenomas for each phage clone was analyzed using flow cytometry [Fig. 3(b)]. A common 7-mer phage that expresses the sequence HAIYPRH is a known contaminant and was run [labeled # in Fig. 3(b)] to ensure the validity of the assay.[31] The T/B ratio for clone HAIYPRH was found to be 1.10 ± 0.08, indicating minimal binding from a nonspecific clone, as expected. Six phage clones with a T/B ratio (target to wild-type phage) <1.9 were identified as ALTPTPP, NLVNLLP, ANYPREP, ATTVPAS, LTTHYKL, and AKPGYLS [labeled * in Fig. 3(b)]. In addition, the KCCFPAQ peptide was previously found to bind to human HT29 cells.[32] These seven peptides were synthesized and conjugated to 5′-FITC for evaluation of in vivo binding. In addition, the GGGAGGG peptide was used as a control. In vivo imaging of the eight

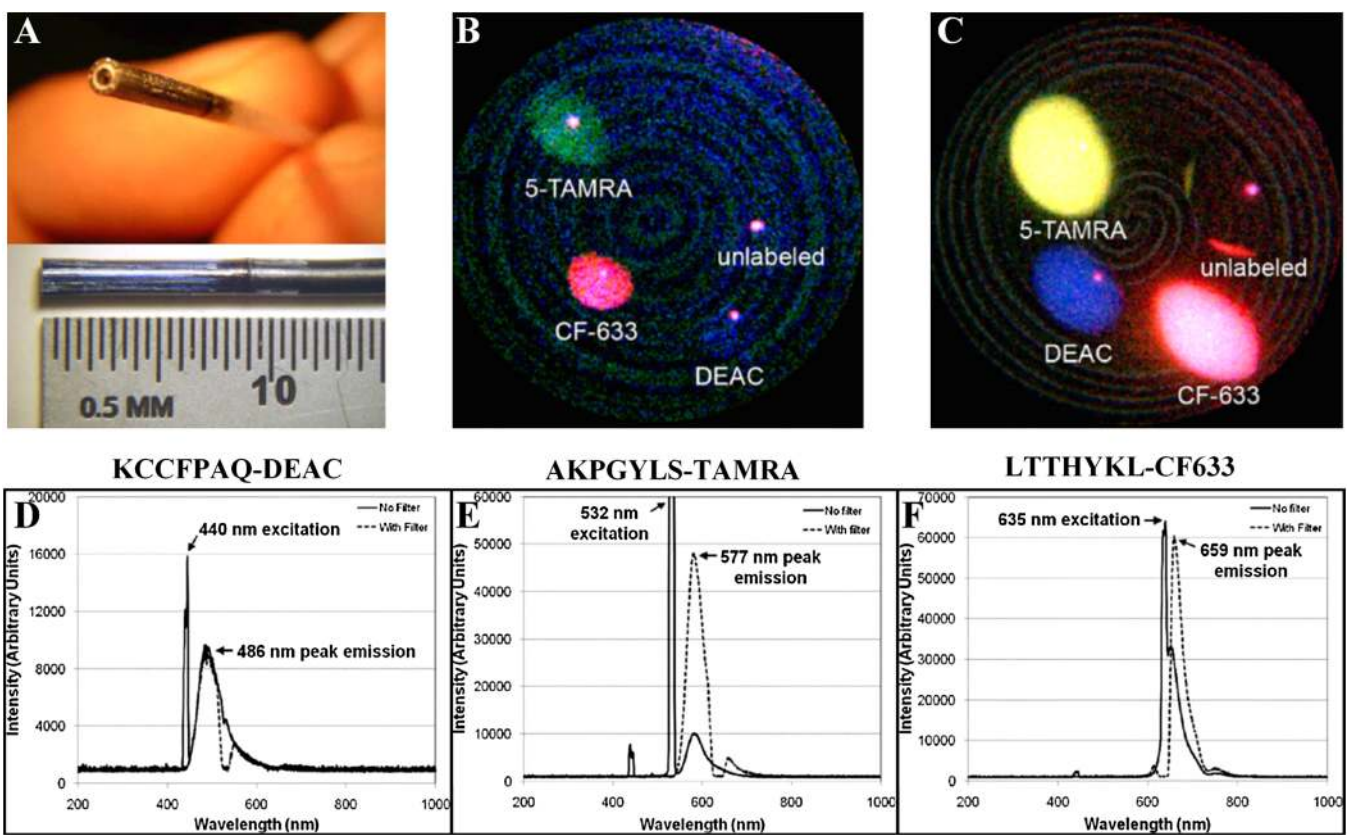

Fig. 2 Multispectral performance. (a) En face (top) and side-view (bottom) of distal tip of multispectral scanning fiber endoscope with 1.6 mm outer diameter and 10 mm rigid distal tip. Single video-frame image of droplets of peptides labeled with DEAC (blue), TAMRA (green/yellow), and CF633 (red) at (b) 1 μM and (c) 100 μM. Unlabeled peptide shows no signal (only specular reflection). Spectra of the fluorescent-labeled peptides labeled with (d) KCCFPAQ-DEAC, (e) AKPGYLS-TAMRA, and (f) LTTHYKL-CF633 at 1 μM concentration with (dashed lines) and without (solid lines) excitation filters show minimal overlap (crosstalk) among the fluorescence emission bands for the three peptides and small shifts (9 to 14 nm) in the peak emission wavelength of the dye after peptide labeling.

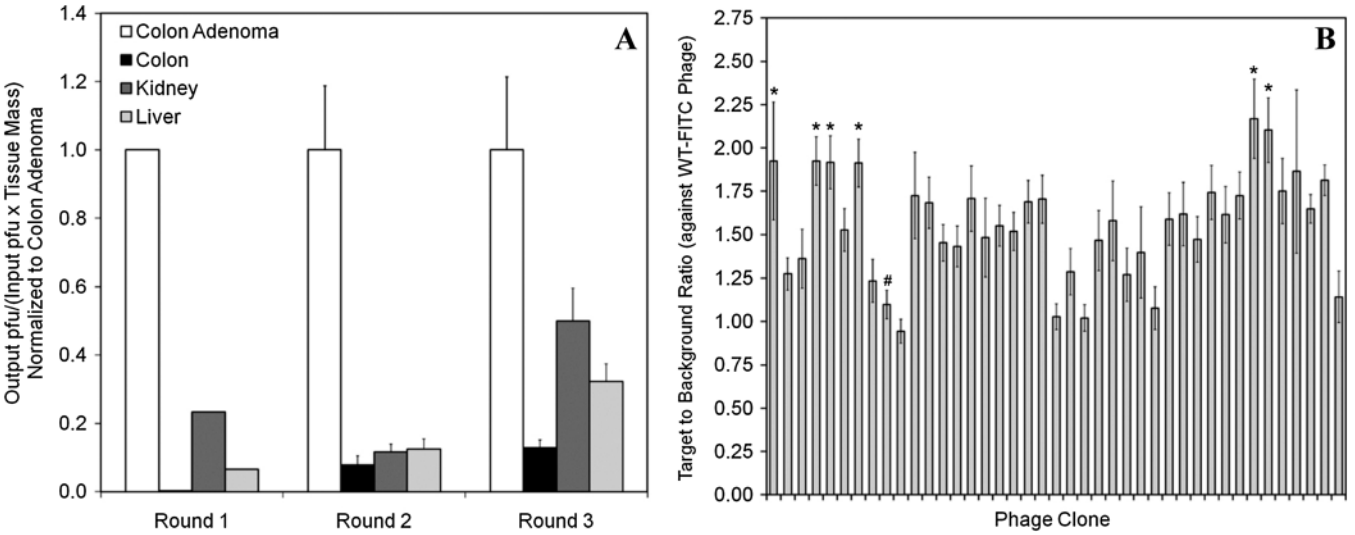

Fig. 3 In vivo phage biopanning results. (a) Counts of phage bound to murine colon adenomas compared normal to colon, kidney, and liver tissue show preferential binding to adenomas. (b) Flow cytometry of 5′-FITC labeled phages binding to isolated colonic adenoma epithelial cells compared to a wild-type phage. Each phage was tested in duplicate. An asterisk (*) indicates a phage clone with a $T/B > 1.9$ that was synthesized for in vivo testing. The pound (#) indicates the clone HAIYPRH used as a control.

FITC-labeled peptides with the nonscanning endoscope demonstrated that KCCFPAQ, AKPGYLS, and LTTHYKL exhibited the highest T/B ratio for binding to colonic adenomas in vivo, shown in Table 1. These three peptides were subsequently conjugated to DEAC, TAMRA, and CF633, respectively, for in vivo imaging with the multispectral scanning fiber endoscope. The control peptides GGGAGGGAGGGK (DEAC)-NH_2 and GGGAGGGAGGGK (5-TAMRA)-NH_2 were also synthesized.

Table 1 Summary of imaging results. The average T/B ratios for in vivo imaging of colonic adenomas in *CPC;Apc* mice are shown for candidate peptides labeled with FITC for validation of specific binding using a nonscanning endoscope and for target peptides labeled with DEAC and TAMRA using the multispectral scanning fiber endoscope.

Nonscanning endoscopy results			
Peptide	*n* (mice)	*n* (adenomas)	Average T/B
KCCFPAQ-FITC	3	9	1.69 ± 0.70
AKPGYLS-FITC	4	7	1.53 ± 0.48
LTTHYKL-FITC	5	13	1.50 ± 0.73
ALTPTPP-FITC	3	10	1.19 ± 0.18
ATTVPAS-FITC	2	3	1.06 ± 0.33
NLVNLLP-FITC	1	2	0.99 ± 0.06
ANYPREP-FITC	1	2	0.94 ± 0.11
GGGAGGG-FITC	3	13	1.05 ± 0.05
Multispectral scanning fiber endoscopy results			
Peptide	*n* (mice)	*n* (adenomas)	Average T/B
KCCFPAQ-DEAC	3	7	1.71 ± 0.19
AKPGYLS-TAMRA	3	6	1.67 ± 0.12
GGGAGGG-DEAC	2	4	1.19 ± 0.09
GGGAGGG-TAMRA	2	4	1.32 ± 0.10

3.3 *Fluorescence Images from Multiple Peptides*

Images of the droplets of KCCFPAQ-DEAC, AKPGYLS-TAMRA, LTTHYKL-CF633, and an unlabeled peptide on a cover glass shown in Fig. 2 demonstrate the capability of the multispectral scanning fiber endoscope to simultaneously detect multiple peptides conjugated to various fluorophores over the visible spectrum. Droplets at concentrations of 1 μM [Fig. 2(b)] and 100 μM [Fig. 2(c)] were imaged to span the typical range used in vivo, indicating that this instrument has the capability of detecting microMolar peptide concentrations. A red-shift in color of fluorescence from the 5-TAMRA droplet (green to yellow) appears to occur with increased concentration. The single bright spots on each droplet represent specular reflections of the laser illumination that change in position with the orientation of the distal tip of the endoscope.

3.4 *Fluorescence Spectra from Multiple Peptides*

The excitation and emission spectra of the three RGB laser sources and fluorescent-labeled peptides over the visible spectrum measured with the fiber coupled spectrophotometer are shown in Fig. 2. The spectra were collected from the labeled peptides both with (dashed line) and without (solid line) use of the respective dichroic (bandpass) filters ($\lambda_{R,G,B}$). In Fig. 2(d), excitation at 440 nm and peak emission at 486 nm are shown for the KCCFPAQ-DEAC peptide. In Fig. 2(e), excitation at 532 nm and peak emission at 577 nm are shown for the AKPGYLS-TAMRA peptide. In Fig. 2(f), excitation at 635 nm and peak emission at 659 nm are shown for the LTTHYKL-CF633 peptide. These spectra show minimal overlap (crosstalk) among the fluorescence emission bands for the three peptides. Moreover, these results show that labeling the peptide with an organic dye causes only a small shift (9 to 14 nm) in the peak emission wavelength.

3.5 *Individually Targeted In Vivo Images*

Images collected with the fluorescent-labeled peptides a) KCCFPAQ-DEAC, b) AKPGYLS-TAMRA, and c) LTTHYKL-CF633 administrated individually are shown [Figs. 4(a)–4(c)]. Specific binding of each peptide to colonic dysplasia (arrows) is demonstrated by comparing the

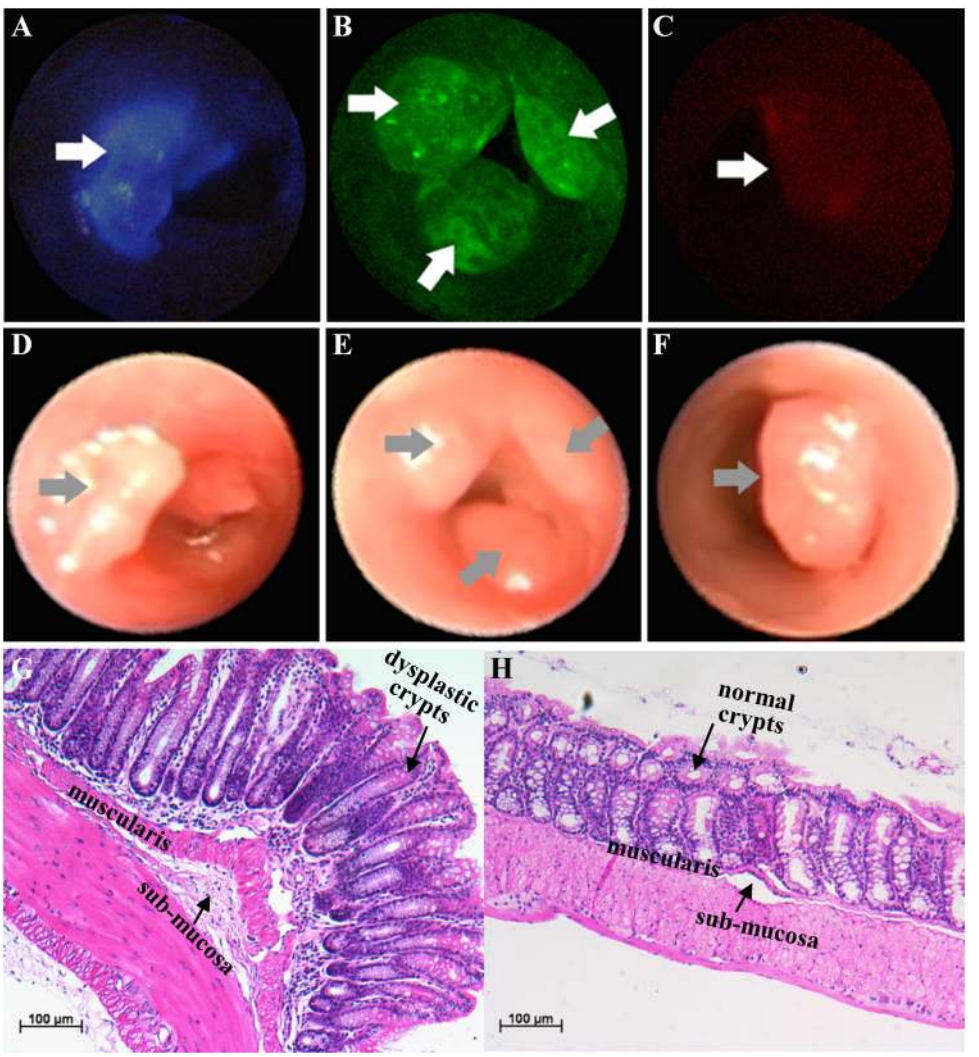

Fig. 4 Individually targeted in vivo images. Colonic adenomas (arrows) are localized on wide-field fluorescence images collected with the multispectral endoscope using separately administered peptides (a) KCCFPAQ-DEAC, (b) AKPGYLS-TAMRA, and (c) LTTHYKL-CF633. The corresponding white light images are shown in (d–f). Routine histology (H&E) of (g) adenoma shows features similar to those seen in sporadic human adenomas, including enlarged nuclei, hyperchromaticity, and distorted crypt architecture, and (h) normal appearing adjacent colonic mucosa, scale bar 100 μM

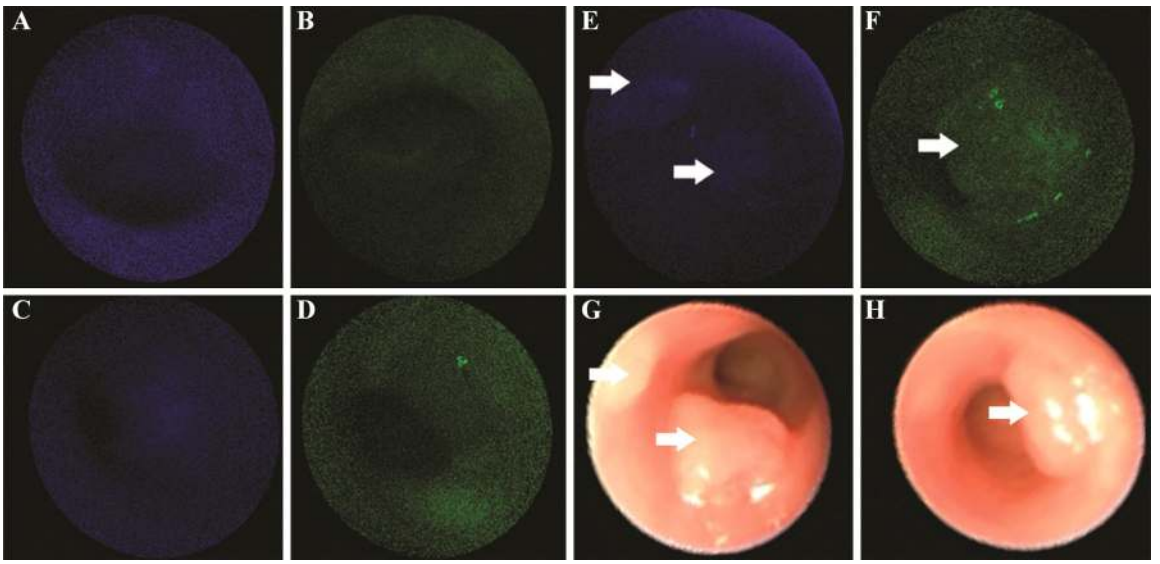

Fig. 5 Minimal nonspecific binding. After administration of (a) KCCFPAQ-DEAC and (b) AKPGYLS-TAMRA to normal colonic mucosa, minimal signal is seen, a result comparable to that found with no administration of peptide (autofluorescence) for the (c) blue and (d) green channels. Minimal signal is seen as well for binding of the control peptides (e) GGGAGGG-DEAC and (f) GGGAGGG-TAMRA to the adenomas (arrows).The corresponding white light images for (e) and (f) are shown in (g) and (h)

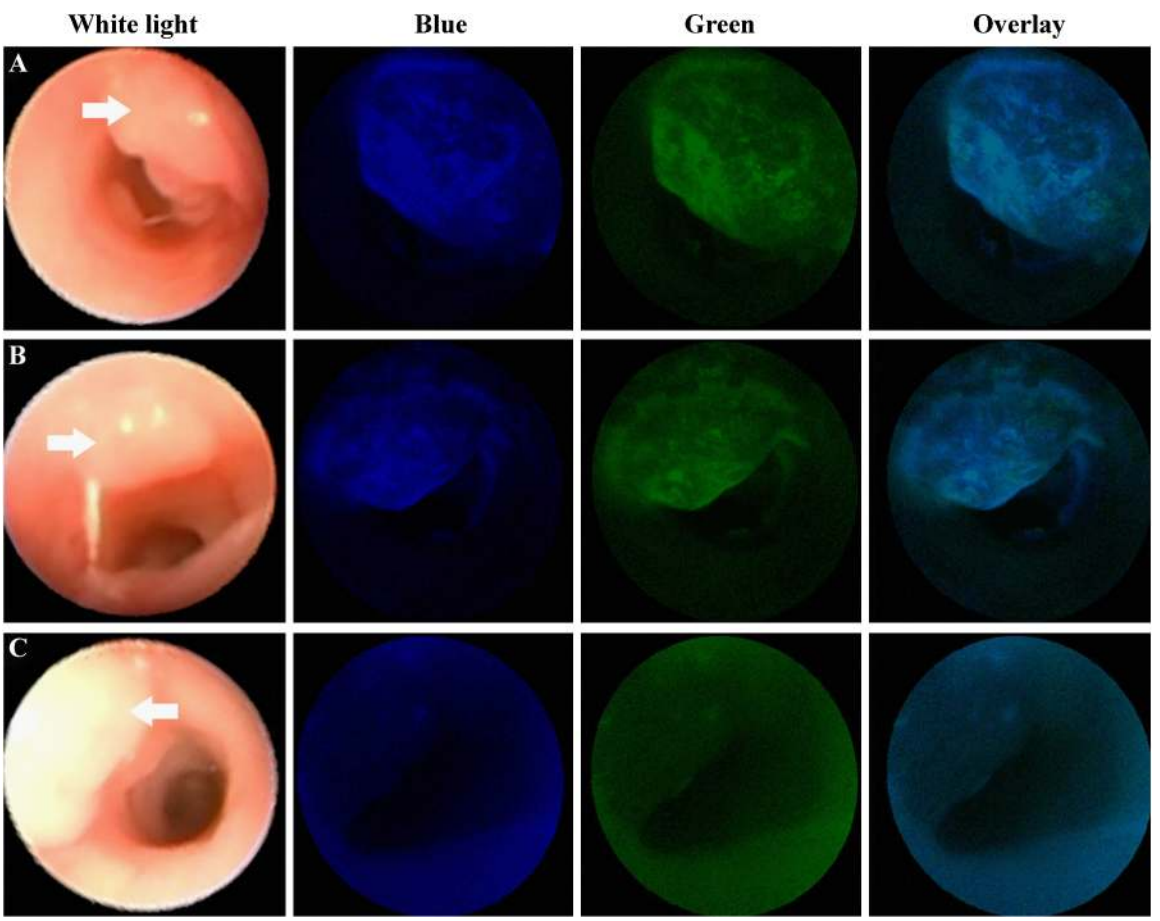

Fig. 6 Combined targeted in vivo images. White light images from different colonic adenomas are shown in the left column. (a) and (b) Administration of the KCCFPAQ-DEAC and AKPGYLS-TAMRA peptide sequentially results in separate spatial patterns of binding to colonic dysplasia in the blue and green channels, as shown by the overlay image. Sequential delivery of the (c) control peptides GGGAGGG-DEAC and GGGAGGG-TAMRA resulted in similar intensity to that found for autofluorescence where no peptide was administered.

fluorescence images with the corresponding white light images collected with the nonscanning endoscope shown in the panels directly below [Figs. 4(d)–4(f)]. The lesion margins on fluorescence appear to be sharp in comparison to those on the white light images. The fluorescent-labeled peptides KCCFPAQ-DEAC and AKPGYLS-TAMRA clearly displayed specific binding to colonic dysplasia, while that for the LTTHYKL-CF633 peptide appears to be more subtle. The average T/B ratios of peptide binding to dysplasia versus normal appearing adjacent colonic mucosa were 1.71 ± 0.19 (range 1.50–2.06) and 1.67 ± 0.12 (1.50–1.78) for KCCFPAQ-DEAC and AKP-GYLS-TAMRA, respectively (Table 1), while that for LTTHYKL-CF633 was not measured because of low signal level. Representative histology (H&E) of the adenoma and adjacent normal appearing mucosa is shown in Figs. 4(g) and 4(h), respectively, scale bar 100 μM. The dysplastic crypts show features, such as enlarged nuclei, disorganization, hyperchromaticity, crowded lamina propria, and distorted architecture, similar to those seen in human sporadic adenomas.

In Fig. 5, administration of (a) KCCFPAQ-DEAC and (b) AKPGYLS-TAMRA to normal colonic mucosa resulted in minimal signal, a result comparable to that found with no administration of peptide (autofluorescence) seen in the (c) blue and (d) green channels. Also, minimal signal is seen for binding of the control peptides (e) GGGAGGG-DEAC and (f) GGGAGGG-TAMRA to the adenomas (arrows), resulting in T/B ratios of 1.19 ± 0.09 and 1.32 ± 0.10 (Table 1), respectively. The corresponding white light images for (e) and (f) are shown in panels (g) and (h). Statistical differences between the target and control peptides for KCCFPAQ and AKPGYLS were $p = 0.009$ and $p = 0.001$, respectively. A quantitative comparison of fluorescence intensities for binding of the control peptide to adenomas and autofluorescence (no peptide) could not be made because the effect on the low signal levels by the system autogain function.

3.6 *Combined Targeted In Vivo Images*

White light images of colonic adenomas from three different mice are shown along the first column in Fig. 6. Sequential administration of the KCCFPAQ-DEAC and AKPGYLS-TAMRA peptides results in separate spatial patterns of binding to colonic dysplasia in the blue and green channels, as shown by the overlay image in Figs. 6(a) and 6(b). This result suggests that each peptide binds to a different cell surface target. Combined delivery of the control peptides GGGAGGG-DEAC and GGGAGGG-TAMRA resulted in similar intensity to that found for autofluorescence where no peptide was administered, shown in Fig. 6(c).

4 Discussion

Here, we demonstrate a flexible, fiber optic endoscope that can image multiple fluorescent-labeled peptides in vivo both independently and simultaneously over large mucosal surface areas in real time. This enabling technology has potential to be used to localize the presence of dysplasia for early colorectal cancer detection, improve the precision of tumor margin detection for endoscopic mucosal resection, and monitor clonal evolution of individual progenitors. While three channels were demonstrated in this study, this optical design can be adapted for use with several more colors by using other fluorescent dyes with nonoverlapping emission bands in the visible and near-infrared regime. Multispectral images can be collected to distinguish the contribution of individual over-expressed gene targets by examining unique spatial expression patterns, a technique that is promising for studying epigenetic and environmental factors that influence cancer formation in mice that are genetically identical at birth. Moreover, this information can be used in the future to perform personalized image-guided therapy. The small size of the instrument allows for its use as an adjunct to standard medical endoscopes. To the best of our knowledge, this is the first report of a miniature, endoscope-compatible instrument that can concurrently image multiple molecular probes in different spectral regimes in vivo.

Previously, we identified the QPIHPNNM peptide using an in vivo biopanning strategy with a T7 18-mer combinatorial phage library. This peptide was used to demonstrate feasibility for performing wide-field fluorescence imaging in vivo using nonscanning endoscopy[19] and microendoscopy.[33] The SFE offers a wide-field view with 6× better resolution than comparable flexible endoscopes that use a fiber-optic bundle.[26] To identify additional peptides that preferentially bind to colonic dysplasia in the mouse, the M13 7-mer phage display library was used to isolate candidate clones. While the *T*7 bacteriophage system has advantages over the *M*13, such as less amplification bias, the 18-mer peptides were more difficult to consistently synthesize and conjugate to a variety of fluorophores. As a result, we chose to pursue the 7-mer *M*13 system to isolate peptide candidates to evaluate the multispectral system. Furthermore, we used engineered mice that are genetically identical, and we do not expect much variation in target expression. Thus, we kept the number of animals used in this study to a minimum for demonstrating proof-of-concept.

We chose the organic dyes DEAC, TAMRA, and CF633 to label the three target peptides because their absorption peaks were close to the excitation wavelengths of the three laser sources. However, there are other dyes available at each wavelength, and we considered other important parameters, including fluorophore solubility, synthesis feasibility, fluorescence at neutral pH, biodistribution, clearance, and potential toxicity for future clinical use, before making our final decision. Moreover, the covalent conjugation of these dyes to the peptide must not affect the binding activity of the targeting moiety. While no clinical data have been reported for use of these dyes, there is reason to believe that each of these fluorophores will be safe for human use, in particular with topical application. Coumarin derivatives have been shown to be safe in a number of preclinical studies.[34,35] TAMRA is structurally similar to fluorescein, an imaging agent that is FDA-approved for human use. The red-shift in fluorescence with increased concentration from the TAMRA-labeled peptide likely results from a quenching effect, which occurs when more of the shorter wavelengths of fluorescence becomes absorbed with a reduced average distance between dye molecules.[36] We do not expect this shift to introduce crosstalk in the multispectral images because the peptides bind at low concentration. In addition, CF633 belongs to the carbocyanine family along with indocyanine green, another FDA-approved dye.

The T/B ratios found for KCCFPAQ-DEAC and AKP-GYLS-TAMRA with the multispectral system are consistent with those found for KCCFPAQ-FITC and AKPGYLS-FITC obtained with the nonscanning endoscope, validating

AKPGYLS and KCCFPAQ as specific binding peptides for colonic dysplasia. In the fluorescence images, a difference in background from nonspecific binding of the target peptides to normal mucosa and from autofluorescence (no peptide) was unnoticeable. The T/B ratio for binding of the GGGAGGG (control) peptide to adenomas was found to be <1, suggesting that some nonspecific binding may have occurred. The LTTHYKL-CF633 peptide did not achieve results comparable to LTTHYKL-FITC, suggesting that another dye may be needed for future studies. Alternatively, the detector in the red channel may not have sufficient sensitivity for in vivo imaging, despite our ability to detect the CF633-labeled peptide at 1 μM concentration from the droplet in Fig. 2(b), and may need to be upgraded. Furthermore, development of a compensation algorithm for anatomical and geometrical differences between images, such as orientation of the endoscopy to the adenomas and sidewalls, would allow more accurate comparison of the T/B ratio measurements. The ultrathin dimensions and flexibility of this multispectral endoscope allow for seamless integration with standard instrument channels of conventional medical endoscopes. Moreover, the lasers, detectors, and data acquisition system are conveniently contained within a portable cart that can be easily transported around a procedure room.

These results demonstrate the in vivo use of a multispectral scanning fiber endoscope to collect wide-field fluorescence images in real time from three peptides that are highly specific for dysplasia in a murine model of colorectal cancer. This integrated methodology has the potential to advance early cancer detection and image-guided therapy in human patients by simultaneously visualizing multiple gene targets that are overexpressed in neoplasia. The small size of this instrument allows for endoscope compatibility and for generalizing the future use of this imaging strategy to other hollow organs.

Acknowledgments

We acknowledge funding support from the US National Institutes of Health: U54 CA13642, R01 CA142750, P30 DK34933 (pilot award), P50 CA93990, RC1 EB010900. The authors thank Dr. Gary Luker for training in murine heart perfusion, Chris Komarck for technical support, and Tim Soper for providing the original artwork for Fig. 1.

Appendix: Methods

A1 In Vivo Peptide Selection

A seven-month old *CPC;Apc* mouse was injected via tail vein with 2×10^{11} pfu of the parent M13-7mer Ph.D.7™ Phage Display Library (New England Biolabs, Beverly, MA). The library was allowed to circulate for 10 min, after which the mouse was euthanized by carbon dioxide asphyxiation and immediately heart-perfused with phosphate buffer solution with protease inhibitors (PBS-PI): 1 mM phenylmethanesulfonylfluoride (PMSF), 20 μg/mL aprotinin, and 1 μg/mL leupeptin). Organs were extracted after perfusion and kept on ice. The bound phages were recovered by homogenizing each tissue or organ (Bio-gen Pro 200) in DMEM-PI (Dulbecco's Modified Eagle Medium plus protease inhibitors: 1 mM phenylmethanesulfonylfluoride (PMSF), 20 μg/mL aprotinin, and 1 μg/mL leupeptin). The tissue samples were washed three times with ice-cold washing medium (DMEM-PI containing 1% bovine serum albumin (BSA)), centrifuging for 5 min at 3000 rpm between each wash. After the last wash, freshly starved *Escherichia coli* (ER2738) were added to each tissue homogenate and incubated for 30 min at room temperature (RT). Prewarmed Luria-Bertani (LB) medium was then added to the bacteria-homogenate solution and incubated for an additional 30 min at RT. The supernatant was recovered after centrifugation and tittered to determine the number of bound phage within each tissue tested. This procedure constituted one round of biopanning. A total of three rounds of phage biopanning were performed, with amplification of the recovered eluate after each biopanning round. The input phage number (2×10^{11} pfu) was kept constant for each round of biopanning. Tittering was performed with appropriate serial dilutions for both eluted phage and amplified phage after each round of biopanning. Agar plates treated with IPTG (isopropyl-b-D-thiogalactosidase) and Xgal (5-bromo-4-chloro-3-indoyl-b-D-thiogalactosidase) were able to visually identify plaques using blue/white screening. Amplified phages from selected phage plaques were purified by PEG/NaCl (polyethylene glycol/sodium chloride) precipitation. All M13 DNA was sequenced after isolating single stranded DNA using an iodide buffer extraction via dideoxy chain termination using a DNA sequencer (Applied Biosystems, 3730XL DNA Analyzer, UM DNA Core) with the NEB-96 gIII sequencing primer provided by New England Biolabs (#S1259S). The number of phages bound to each organ or tissue was calculated as the output pfu/(input pfu $\times$ tissue mass).

A2 Flow Cytometry Validation

Primary colon epithelial cells were extracted from freshly excised colon adenomas from euthanized *CPC;Apc* mice. Freshly isolated tissue was minced with sterile razor blades into pieces <1 mm in size and washed with a tissue rinse solution (Hank's balanced salt solution containing 2% glucose, 250 μg/mL Amphotericin B, and 10 μg/mL penicillin-streptomycin). The tissue was centrifuged at 5000 rpm for 3 min, and the supernatant was aspirated. The tissue was washed again and then digested in HBSS containing 2% bovine serum albumin, 60 units/mL collagenase, 0.02 μg/mL dispase I, and 0.2 μg/mL soybean trypsin inhibitor for 18 h at 37 °C. Epithelial cells were separated and collected as a pellet after two rinses with wash media (Dulbucco's medium containing 2% sorbitol, 5% fetal bovine serum, and 10 μg/mL penicillin-streptomycin).

FITC-labeled phage were prepared by combining 1×10^{13} pfu of phage in 200 μL of 1 M Sodium Carbonate conjugation buffer (pH 9.0) with 20 μL of 5 mg/mL FITC in the same conjugation buffer and rotating in the dark for 2 h. Purification and concentration of the phages were accomplished by transferring the solution to Amicon Ultracel 3k centrifugal filters (Millipore UFC800396), adding 3.5 mL of PBS and centrifuging (Eppendorf 5810R) at 4000 rpm and 4 °C for 35 min, discarding the wash and repeating for a total of three times, ending with a total volume of 200 μL of phage solution. The phage solution was tittered to determine end phage concentration.

1×10^7 primary epithelial cells per sample were blocked with PBS containing 1% BSA for 30 min on ice. Cells were centrifuged at 2000 rpm for 5 min and washed twice with PBS containing 1% BSA, centrifuging after each wash. Cells were then incubated with 1×10^{10} FITC-conjugated phages of each individual clone being tested in PBS for 1 h on ice with gentle shaking. Cells were subsequently washed in PBS with 1% BSA three times, centrifuging after each wash. Cells were resuspended in PBS and immediately analyzed on

Table 2 Peptide characterization, including % purity on HPLC and calculated versus observed molecular weight (MW) on mass spectrometry.

Peptide-label sequence	% Purity HPLC	Calc MW$(M+H)^+$	Obs MW$(M+H)^+$
AKPGYLS-GGGSK-(5-FITC)-NH_2	96.3	1509.8	1509.6
KCCFPAQ-GGGSK-(5-FITC)-NH_2	99.1	1570.6	1570.4
LTTHYKL-GGGSK-(5-FITC)-NH_2	96.9	1649.9	1649.7
ALTPTPP-GGGSK-(5-FITC)-NH_2	98.9	1470.5	1471.1
ATTVPAS-GGGSK-(5-FITC)-NH_2	93.3	1420.4	1420.6
NLVNLLP-GGGSK-(5-FITC)-NH_2	97.3	1556.6	1556.7
ANYPREP-GGGSK-(5-FITC)-NH_2	99.4	1620.6	1621.2
GGGAGGGAGGGK-(5-FITC)-NH_2	99.5	1189.3	1189.5
KCCFPAQ-GGGSK-(DEAC)-NH_2	98.5	1424.7	1424.5
GGGAGGGAGGGK-(DEAC)-NH_2	97.8	1044.3	1044.4
AKPGYLS-GGGSK-(5-TAMRA)-NH_2	97.0	1532.8	1532.6
GGGAGGGAGGGK-(TAMRA)-NH_2	98.4	1213.3	1213.4
LTTHYKL-GGGSK-(CF633)-NH_2	98.8	2062.6	2063.9

a FACSDiVa flow cytometer (BD® LSRII, BD Biosciences, San Jose, CA; FlowJo Analysis Software, Tree Star Inc., Ashland, OR). A wild-type phage containing no peptide insert was labeled with FITC and used as a control. Forty-two independent phage clones were tested in duplicate. T/B ratios against the wild-type FITC-phage clone were calculated as: Mean FITC value of candidate phage/Mean FITC value of wild-type phage. The top six phages having the highest T/B ratios were further synthesized as peptides for preliminary testing in vivo.

A3 Small Animal Endoscopy Validation

Prior to peptide administration, the colon of each animal was prepped using a tap water lavage. Using a nonscanning endoscope (Karl Storz Veterinary Endoscopy, Goleta, CA) with a 3 Fr instrument channel for peptide administration, adenomas suitable for imaging were located, and the colon was rinsed with water until all of the visible mucous was removed. The fluorescence-labeled peptides were delivered at a concentration of 100 μM in 1 × PBS through the instrument channel, as previously described.[19] Adenomas in *CPC;Apc* mice developing distal colonic adenomas were imaged with both white light and fluorescence endoscopy. Mean values (arbitrary units) were calculated for each ROI, and a T/B ratio for the adenoma/normal-appearing adjacent colonic mucosa was then calculated for each adenoma and averaged for each peptide (Table 2). The top three peptides with the greatest T/B ratios were then labeled with visible fluorophores (DEAC, 5-TAMRA, and CF633) for imaging with the SFE.

References

1. D. Heresbach et al., "Miss rate for colorectal neoplastic polyps: a prospective multicenter study of back-to-back video colonoscopies," *Endoscopy* **40**(4), 284–290 (2008).
2. J. C. van Rijn et al., "Polyp miss rate determined by tandem colonoscopy: a systematic review," *Am. J. Gastroenterol.* **101**(2), 343–350 (2006).
3. D. K. Rex et al., "Colonoscopic miss rates of adenomas determined by back-to-back colonoscopies," *Gastroenterology* **112**(1), 24–28 (1997).
4. A. Parra-Blanco et al., "Risk for high-grade dysplasia or invasive carcinoma in colorectal flat adenomas in a Spanish population," *Gastroenterol. Hepatol.* **29**(10), 602–609 (2006).
5. K. Togashi et al., "Flat and depressed lesions of the colon and rectum: pathogenesis and clinical management," *Ann. Acad. Med. Singapore* **32**(2), 152–158 (2003).
6. M. J. O'Brien et al., "National Polyp Study Workgroup. Flat adenomas in the National Polyp Study: Is there increased risk for high-grade dysplasia initially or during surveillance?," *Clin. Gastroenterol. Hepatol.* **2**(10), 905–911 (2004).
7. G. Gualco et al., "Flat elevated lesions of the colon and rectum: a spectrum of neoplastic and nonneoplastic entities," *Ann. Diagn. Pathol.* **10**(6), 333–338 (2006).
8. B. K. Edwards et al., "Annual report to the nation on the status of cancer, 1975–2006, featuring colorectal cancer trends and impact of interventions (risk factors, screening, and treatment) to reduce future rates," *Cancer* **1**(116(3)), 544–573 (2010).
9. H. Alencar et al., "Colonic adenocarcinomas: near-infrared microcatheter imaging of smart probes for early detection—study in mice," *Radiology* **244**(1), 232–238 (2007).
10. J. Cardoso et al., "Expression and genomic profiling of colorectal cancer," *Biochim. Biophys. Acta.* **1775**(1), 103–137 (2007).
11. M. van Oosten et al., "Selecting potential targetable biomarkers for imaging purposes in colorectal cancer using TArget Selection Criteria (TASC): a novel target identification tool," *Trans. Oncol.* **4**(2), 71–82 (2011).
12. C. H. Tung et al., "In vivo imaging of proteolytic enzyme activity using a novel molecular reporter," *Cancer Res.* **60**(17), 4953–4958 (2000).
13. C. Bremer et al., "Optical imaging of matrix metalloproteinase-2 activity in tumors: feasibility study in a mouse model," *Radiology* **221**(2), 523–529 (2001).
14. H. W. Kang et al., "Targeted imaging of human endothelial-specific marker in a model of adoptive cell transfer," *Lab. Invest.* **86**(6), 599–609 (2006).

15. B. Laxman et al., "Noninvasive real-time imaging of apoptosis," *Proc. Natl. Acad. Sci. U.S.A.* **99**(26), 16551–16555 (2002).
16. S. M. Messerli et al., "A novel method for imaging apoptosis using a caspase-1 near-infrared fluorescent probe," *Neoplasia* **6**(2), 95–105 (2004).
17. P. L. Hsiung et al., "Detection of colonic dysplasia in vivo using a targeted heptapeptide and confocal microendoscopy," *Nat. Med.* **14**(4), 454–458 (2008).
18. M. Li et al., "Affinity peptide for targeted detection of dysplasia in Barrett's esophagus," *Gastroenterology* **139**(5), 1472–1480 (2010).
19. S. J. Miller et al., "In vivo fluorescence-based endoscopic detection of colon dysplasia in the mouse using a novel peptide probe," *PLoS One* **6**(3), e17384 (2011).
20. E. Dekker et al., "Narrow-band imaging compared with conventional colonoscopy for the detection of dysplasia in patients with longstanding ulcerative colitis," *Endoscopy* **39**(3), 216–221 (2007).
21. K. Gono et al., "Appearance of enhanced tissue features in narrow-band endoscopic imaging," *J. Biomed. Opt.* **9**(3), 568–577 (2004).
22. A. Adler et al., "A prospective randomised study on narrow-band imaging versus conventional colonoscopy for adenoma detection: does narrow-band imaging induce a learning effect?" *Gut* **57**(1), 59–64 (2008).
23. M. G. Lapalus et al., "Does chromoendoscopy with structure enhancement improve the colonoscopic adenoma detection rate?," *Endoscopy* **38**(5), 444–448 (2006).
24. N. Uedo et al., "Diagnosis of colonic adenomas by new autofluorescence imaging system: a pilot study," *Digest. Endosc.* **19**(S1), S134–S138 (2007).
25. T. D. Wang et al., "In vivo identification of colonic dysplasia using fluorescence endoscopic imaging," *Gastrointest. Endosc.* **49**(4 Pt 1), 447–455 (1999).
26. E. J. Seibel et al., "Tethered capsule endoscopy, a low-cost and high-performance alternative technology for the screening of esophageal cancer and Barrett's esophagus," *IEEE Trans. Biomed. Eng.* **55**(3), 1032–1042 (2008).
27. C. M. Lee et al., "Scanning fiber endoscopy with highly flexible, 1 mm catheterscopes for wide-field, full-color imaging," *J. Biophoton.* **3**(5–6), 385–407 (2010).
28. T. Hinoi et al., "Mouse model of colonic adenoma-carcinoma progression based on somatic Apc inactivation," *Cancer Res.* **67**(20), 9721–9730 (2007).
29. E. J. Seibel et al., "Scanning single fiber endoscopy: a new platform technology for integrated laser imaging, diagnosis, and future therapies," *Gastrointest. Endosc. Clin. N. Am.* **18**(3), 467–478 (2008).
30. C. N. Arnold et al., "Molecular pathogenesis of colorectal cancer: implications for molecular diagnosis," *Cancer* **104**(10), 2035–2047 (2005).
31. L. A. Brammer et al., "A target-unrelated peptide in an M13 phage display library traced to an advantageous mutation in the gene II ribosome-binding site," *Anal. Biochem.* **373**(1), 88–98 (2008).
32. B. P. Joshi et al., "Fluorescence detection of colonic neoplasia using a novel peptide," *Gastroenterology* **140**(S1), S-341 (2011).
33. S. F. Elahi et al., "Targeted imaging of colorectal dysplasia in living mice with fluorescence microendoscopy," *Biomed. Opt. Express* **2**(4), 981–986 (2011).
34. X. Chen et al., "Attenuation of experimental autoimmune encephalomyelitis in C57 BL/6 mice by osthole, a natural coumarin," *Eur. J. Pharmacol.* **629**(1–3), 40–46 (2010).
35. K. Watanabe et al., "In vivo imaging of zebrafish retinal cells using fluorescent coumarin derivatives," *BMC Neurosci.* **11**(1), 116 (2010).
36. M. Fikry, M. M. Omar, and L. Z. Ismail, "Effect of host medium on the fluorescence emission intensity of rhodamine B in liquid and solid phase," *J. Fluoresc.* **19**(4), 741–746 (2009).